Construction and Building Materials 292 (2021) 123393

Contents lists available at ScienceDirect

Construction and Building Materials

journal homepage: www.elsevier.com/locate/conbuildmat

Influence of Portland cement and alkali-activated slag binder on the thermoelectric properties of the p-type composites with MWCNT

Hyeong Min Park [a,b], Solmoi Park [c], In-Jin Shon [b], G.M. Kim [d], Sunbin Hwang [e], Min Wook Lee [e], Beomjoo Yang [a,*]

[a] School of Civil Engineering, Chungbuk National University, 1 Chungdae-ro, Seowon-gu, Cheongju, Chungbuk 28644, Republic of Korea
[b] Division of Advanced Materials Engineering, Jeonbuk National University, 567 Baekje-daero, Deokjin-gu, Jeonbuk 54896, Republic of Korea
[c] Department of Civil Engineering, Pukyong National University, 45 Yongso-ro, Nam-gu, Busan 48513, Republic of Korea
[d] Korea Institute of Geoscience and Mineral Resources, 124 Gwahak-ro, Yuseong-gu, Daejeon 34132, Republic of Korea
[e] Institute of Advanced Composite Materials, Korea Institute of Science and Technology (KIST), 92 Chudong-ro, Bongdong-eup, Wanju-gun, Jeonbuk 55324, Republic of Korea

HIGHLIGHTS

- The thermoelectric properties of p-type cementitious composites with CNT were studied.
- The Portland cement and alkali-activated slag materials were considered as binder materials.
- The various contents of MWCNT was utilized as the conductive filler.
- This is the first study on thermoelectric research of proposed cementitious composites.

GRAPHICAL ABSTRACT

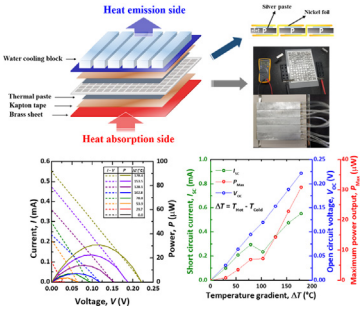

ARTICLE INFO

Article history:
Received 23 November 2020
Received in revised form 30 March 2021
Accepted 13 April 2021
Available online 30 April 2021

Keywords:
P-type thermoelectric material
Portland cement
Blast furnace slag
Electrical resistivity
Thermal conductivity
Multi-walled carbon nanotube

ABSTRACT

Herein, we introduce p-type thermoelectric materials composed of Portland cement (PC) and slag-based alkali-activated cement (AAC) composites containing multi-walled carbon nanotube (MWCNT). Numerous characteristics related to the thermoelectric properties, in this case the electrical conductivity, compressive strength, thermal conductivity, Seebeck coefficient, and power factor of composites composed of two types of binders, were investigated, and various physicochemical properties were analyzed to determine their enhancement mechanisms. Based on the initial test results, MWCNT-embedded AAC composites were found to be feasible as a thermoelectric material, and an AAC thermoelectric module containing 2.0 wt% MWCNT was therefore additionally fabricated. The AAC-based thermoelectric module was tested with regard to its energy-harvesting performance, with the result confirming that the module was capable of generating electrical power.

1. Introduction

At present, multifunctional construction materials are commonly researched as a core element for use in the construction of future smart buildings. Portland cement (PC) has long played a prominent role in the construction field; however, in relation to the production of PC, there is growing concern about environmental issues associated with global warming, and there have been many efforts to reduce carbon dioxide (CO_2) emissions. The kiln process, one means by which to manufacture PC, generates a large amount of CO_2, representing approximately 8% of all CO_2 emitted into the atmosphere [1,2].

* Corresponding author.
E-mail address: byang@cbnu.ac.kr (B. Yang).

https://doi.org/10.1016/j.conbuildmat.2021.123393
0950-0618/

Alkali-activated cement (AAC) is a cement-like material derived from waste or industrial by-products such as fly ash, and granulated blast furnace slag (GBFS) [3]. Specifically, GBFS, sourced from the ironworks industry, is commercially deployed in various construction fields and is known to be a good alternative to PC, as alkali-activated binders can reduce CO_2 emissions compared to the amounts generated by PC. Hence, many researchers have studied materials capable of replacing PC with GBFS-based AAC for use in the construction field. In an effort to improve its use in eco-friendly, zero-waste, and smart building applications, the importance of research on AAC-based multifunctional construction materials is increasing.

The application of an electrically conductive filler for use in cement-based composites to provide electrical properties has attracted substantial interest. *Nam et al.* [4] *and Kim et al.* [5] *investigated the electrical properties of cementitious composites with an electrically conductive filler material (multi-walled carbon nanotube, MWCNT).* Their experimental results demonstrated that CNT-incorporated cementitious composites are useful for electromagnetic wave shielding and piezoresistive energy harvesting applications. Wei et al. also reported the thermoelectric characteristics of carbon nanotube (CNT)-incorporated cement-based composites [6]. According to their study, the maximum power factor was approximately 57.98 μV/°C at T_{hot} = 75 °C and T_{cold} = 35 °C ($\Delta T = 40$ °C) when the CNT content was 15 wt%. *It was believed that the AAC has a higher fire resistance than PC, the thermoelectric performance was tested at a higher temperature than the previous paper.* In addition, 15 wt% of MWCNT is very high in general, and such a high amount can be a serious disadvantage in terms of cost, viscosity, and workability. In a study by Tzounis et al. [7], for the same reason, the T_{hot} value and temperature gradient were limited to 50 °C and 25 °C, respectively [7].

GBFS-based AAC material can offer good mechanical properties, fire resistance, and good durability. Based on the unique properties of AAC, which differ from those of cement, this material recently has been widely used in construction projects such as pavement applications, retaining walls, water tanks, and precast bridge decks [8]. Most studies of AAC have concentrated on the mechanical properties, and only a few have investigated functional AAC with nanofillers [9–11]. *Collins and Sanjayan have been focused on the mechanical properties of alkali activated slag concrete* [9]. *Marjanović et al. and Çelikten et al. also reported the mechanical and microstructural properties of alkali-activated fly ash-slag mortars* [10,11]. There are no references to the thermoelectric characteristics of AAC/MWCNT composites, despite their strong potential for use as a thermoelectric material given the good heat resistance of these materials [12]. In addition, no comprehensive studies of the mechanical/thermal/electrical properties of PC binders and AAC binders incorporating MWCNTs have been reported. As the research on functional construction materials remains active, it is very important to clarify the physicochemical characteristics gained when incorporating MWCNT into these two materials.

Many researchers have made great efforts to develop functional construction materials containing carbon nanofillers; however, previous studies mainly focused on improving the mechanical and/or electrical properties of the construction composite by incorporating MWCNT into a cement-based material. Over the past few years, we have sought to find the optimal mixing ratio of conductive cementitious composites in which MWCNTs are properly dispersed in cement binder [13–15]. Kim et al. [13,15] studied the effect of polycarboxyl surfactant and silica fume on MWCNT-embedded cement paste. It was confirmed that the polycarboxyl surfactant causes dispersion of MWCNTs due to surface functionalization, and silica fume also causes an additional bearing effect, thereby positively affecting the improvement of MWCNT dispersion. Additionally, the effects of pores and ionized water on electrical conductivity of the composites were experimentally and theoretically *analyzed in* Figs. 5 and 6. It was reported that the ionized water plays the role of electrolytic pore solution and helps to achieve high electrical conductivity of composites in the early stage. However, as the hydration process of the cement progresses, it disappears along with the formation of hydrate phases. Ultimately, it exists as a void over time, resulting in a decrease in electrical conductivity.

From the characteristics and mechanisms introduced earlier, it was able to exhibit various functional characteristics that were difficult to perform in existing cement materials. The accelerated curing [16], monitoring [5], electromagnetic shielding [17], and thermal generation [18] of conductive construction composites are the representative examples. The present study has novelty compared to existing researches in two aspects: (1) Considering both cement and alkali-activated binders, a comprehensive study was conducted on how nanofiller affect the physicochemical properties of each binder. To our knowledge, no studies have been reported so far. (2) The field of applications of conductive construction materials, which was previously limited, has been expanded to thermoelectric. The actual energy harvesting performance was evaluated by fabricating a real-scale module. It was also the content of research that has been conducted quite limitedly in the past, and novel experimental results could be included through the present study.

In this work, PC/MWCNT and AAC/MWCNT composites (each incorporating MWCNT) were fabricated and evaluated to compare various properties of these composites. To investigate the material characteristics of the PC/MWCNT and AAC/MWCNT composites, specimens were fabricated with various mix proportions and exposure temperatures. The p-type thermoelectric characteristics of the specimens were also measured at various temperatures using a ZEM-3 device. An AAC-based thermoelectric module system was then fabricated to evaluate the energy-production capacities of the proposed material.

2. Experimental procedure

2.1. Materials

Class F fly ash (Hadong thermal power plant operated by Korea Southern Power Co., Ltd., South Korea) and GGBS (Hyundai Steel, South Korea) were used as binder materials for the AAC matrix. Type I Ordinary PC (Asia Cement Co., Ltd., South Korea) was also separately prepared as a binder material for comparison purposes. *Slag (Blaine specific surface area = 380 ~ 405 m^2/kg, Specific gravity = 2.85 ~ 3.20* [19]*), Fly ash (Blaine specific surface area = 370 ~ 455 m^2/kg, Specific gravity = 2.35 ~ 245* [20,21]*), and cement (Blaine specific surface area = 420 m^2/kg, Specific gravity = 3.14* [21]*).* The chemical compositions of the binder materials as determined by X-ray fluorescence are shown in Table 1. An alkali activating solution was made by blending sodium hydroxide pellets (Duksan Chemicals Co., South Korea) and a sodium silicate solution (Duksan Chemicals Co., South Korea; Na_2O: 9.2%, SiO_2: 33.3%, H_2O: 57.5%) up to a silicate *m*odulus (SiO_2/Na_2O ratio) of 1.0.

MWCNT produced by the catalytic chemical vapor deposition (CCVD) process was utilized in this study (Jeno Tube 8 ©, JEIO Co., Ltd., South Korea). *The purity, type, length, diameter, bulk density, and BET of the MWCNT were 98.5%, the aligned bundle type, 100–200 μm, 7–9 nm, 0.07–0.09 g/ml, and 400–600 m^2/g respectively (Jeno Tube 8©).* A poly-carboxylic acid-based superplasticizer (GLENIUM 8008, BASF Pozzolith Ltd., Germany) was also utilized in the present test to improve the workability and to disperse the MWCNT.

Table 1
Chemical compositions of the fly ash, GGBS, and Type I Ordinary PC obtained by X-ray fluorescence (wt).

	CaO	SiO_2	Al_2O_3	Fe_2O_3	MgO	Na_2O	K_2O	SO_3	TiO_2	Mn_2O_3	SrO	Sum	LOI*
Fly ash	4.75	56.8	20.8	9.9	1.25	–	1.35	1.0	1.45	–	–	97.3	2.7
Slag	44.8	33.5	13.7	0.5	2.9	0.2	0.5	1.7	0.5	0.2	0.1	98.6	1.4
Portland cement	60.7	20.6	5.2	3.42	2.64	0.11	1.0	2.43	–	0.1	0.1	96.3	3.7

* LOI: Loss on ignition.

2.2. Preparation of specimens

The mix proportions (wt.%) of the AAC/MWCNT and PC/MWCNT specimens are shown in Tables 2 and 3, respectively. The mix proportions in Tables 2 and 3 were converted into the volume ratio, and presetned in Tables A2 and A3, respectively. MWCNT was used as an electrical conductor and was added to the binder with respect to the weight of the binder materials. The amounts of MWCNTs considered in this study were 0.0, 0.3, 0.6, 1.0, 2.0, and 3.0 wt%. *An alkaline activator was obtained by mixing a water 1L, pellet type NaOH 160 g, and Sodium silicate 580 g.* For all specimens, the activator/binder and water/binder ratios were set according to the flow value; these were 111.5 ± 11.5 and 112.5 ± 12.5 mm, respectively. *The increasing of the MWCNT content increases the viscosity of the mixture, making it difficult to fabricate the specimen. The proposed flow value indicates an easy level for casting obtained empirically.*

The procedure used to manufacture the AAC/MWCNT and PC/MWCNT composites is as follows: dry materials, i.e., fly ash and GGBS, or PC were dry-mixed with MWCNT for one minute using a mortar mixer (HJ-1150, Heungjin Testing Machine Co., Ltd., South Korea). The alkali-activating solution or water was added to the mixture, which was then mixed for an additional five minutes. After mixing, the paste mixture was cast into $25 \times 25 \times 25$ mm^3 and $4 \times 4 \times 20$ mm^3 prismatic molds, and both were then sealed with wrapping to prevent the alkaline solution or water from evaporating [16,22,23]. The specimens were cured at an ambient temperature for 3 days and then exposed at four different temperatures of 60, 100, 250, and 400 °C for an additional 24 h.

2.3. Experimental apparatus

The electrical resistance levels of specimens exposed to four different temperatures (60, 100, 250, and 400 ℃) were measured using a digital multimeter (FLUKE-116, Fluke Co., USA), with the measured electrical resistance converted in each case into the electrical resistivity, as follows,

$$\rho = R \cdot \frac{A}{L} \tag{1}$$

where ρ and R denote the electrical resistivity and the electrical resistance, respectively. L is the spacing between the electrodes (cm) and A is the cross-sectional area (cm^2) of the electrode in conjunction with the composite. An instrument manufactured by Hot Disk (TPS-2500 s, Hot Disk Inc., Sweden) in isotropic mode and with a 0.526 mm *k*aption sensor was used to measure the thermal conductivity of each specimen. The compressive strength tests of the composites were done using a UTM (Instron 5985, Instron, Co., USA) at 250 kN according to ASTM C 109 with a cross-head speed of 0.01 mm/s.

Samples for the thermogravimetric analysis *(TGA)* and the X-ray diffraction (XRD) and solid-state nuclear magnetic resonance (NMR) spectroscopy assessments were powdered to pass a 64 μm. *TGA* was conducted using a TGA/DSC1/1600 LF instrument (Mettler-Toledo) at a constant heating rate of 10 °C/min in N_2. The XRD data were recorded using an X'Pert Pro X-ray diffractometer (Malvern Panalytical), a Pixel instrument, and an X'Celerator detector at 40 kV and 30 mA, with a step size of 0.026° 2θ (796.4 s per step). CeO_2 as an external sample was used for the Rietveld refinement-based quantification of the identified minerals and to assess the amorphous phase content. The solid-state ^{29}Si magic-angle spinning (MAS) NMR spectra were obtained using an Avance III HD instrument (9.4 T).

Mercury intrusion porosimetry (MIP) was *conducted* using an AutoPore IV 9500 (Micromeritics Instrument Corporation) device at room temperature and with a contact angle of 130°.

μ-CT and SEM analyses were conducted to investigate the internal structure of the composites with the MWCNT. A μ-CT (SkyScan 1172, Bruker Co., Belgium) analysis with 100 kVp X-rays was also

Table 2
Mix proportion of AAC/MWCNT composite.

Specimen	Slag (g)	Fly ash (g)	MWCNT (wt%)	Alkali activator (g)	Molarity (M)	Flow (mm)
AAC-0	500	500	0	500	8.75	111.5 ± 11.5
AAC-0.3C			0.3	526		
AAC-0.6C			0.6	575		
AAC-1.0C			1.0	625		
AAC-2.0C			2.0	750		
AAC-3.0C			3.0	875		

Table 3
Mix proportion of PC/MWCNT composite.

Specimen	Cement (g)	MWCNT (wt%)	Water (g)	Superplasticizer (g)	Flow (mm)
C-0	1000	0	260	16	112.5 ± 12.5
C-0.3C		0.3	300		
C-0.6C		0.6	350		
C-1.0C		1.0	460		
C-2.0C		2.0	610		
C-3.0C		3.0	800		

used to analyze the internal structure of cylindrical samples (ϕ5 mm and length = 7 mm) with various contents of MWCNT (0, 0.3, 0.6, 1.0, 2.0, and 3.0 wt%). Evaluations were carried out at a camera pixel size of 4 K × 2 K/9 μm and with an Al + Cu filter. For the morphological study using SEM, the composites incorporating MWCNT were dried in an oven at 60 °C for 24 h and then coated with platinum.

In addition, the power factor, Seebeck coefficient, and electrical conductivity of the specimens were measured at various temperatures using a ZEM-3 instrument (M10, ADVANCE RIKO Inc., Japan) to evaluate their potential as thermoelectric devices. Additionally, a semiconductor characterization system (4200-SCS, Keithley Tektronix Inc., USA) was employed to analyze the energy production capacity of the thermoelectric modules.

3. Results and discussion

3.1. Electrical resistivity

Fig. 1 (Table A1) shows the electrical resistivity outcomes of the PC/MWCNT and AAC/MWCNT composites at elevated temperatures. It can be observed that the electrical resistivity of all specimens decreased as the MWCNT content was increased, with no significant decrease in the resistivity observed in the samples when the MWCNT content exceeded 2.0 wt%. This is in agreement with earlier findings [24] that the electrical percolation threshold for cementitious materials incorporating MWCNT is between 0.3 and 0.5 wt% of MWCNT content; hence, no further improvement in the electrical conductivity of cementitious composites could be expected if the MWCNT content had been increased to the range of 2.0–3.0 wt%. Interestingly, similar electrical trends were also observed in the AAC/MWCNT composites.

The electrical resistivity of both the PC/MWCNT and AAC/MWCNT composites did not significantly change from 60 to 250 °C, whereas it significantly increased at 400 °C. It should be noted that some of the samples at elevated temperatures showed exceptionally high electrical resistivity which could not be measured; there outcomes are therefore omitted from Fig. 1. The electrical resistivity data of the AAC/MWCNT composites with an increase in the temperature were generally well measured, while those of the PC/MWCNT composites were not measurable at 400 °C. *AAC is known to be more durable than PC, Especially, fly ash binder has a good fire resistance. The thermally induced phase transformation and the evolution of the porosity of PC composites cause changes in the internal structure, consequently, these changes were adversely affected on the electrical properties of the composite* [25,26].

3.2. Thermal conductivity

The thermal conductivity outcomes with respect to the temperature are presented in Fig. 2 (Table A1). The thermal conductivity of all specimens decreased with an increase in the temperature and MWCNT content. Especially with regard to the PC/MWCNT composites, the reduced range of the thermal conductivity according to the MWCNT content was observed to be greater than that of the AAC/MWCNT composites. The reduction in the thermal conductivity of the composites at an elevated temperature was also more prominent in the PC/MWCNT composites than in the AAC/MWCNT composites. *This result is due to the fact that the degree of decomposition in the AAC binder material as elevated temperature is less than that of the PC binder material. In this regard, the results of thermal analyses are indicated at next section.*

This observation can be explained by the mechanism of heat transport through phonons in materials [27]. The thermal characteristics of anisotropic materials are proportional to the phonon mean-free path, and this is also a dominant factor affecting the thermal conductivity of MWCNT-embedded ceramic composites [28–31]. It is considered that dispersed MWCNTs in the PC and AAC binders could cause interface scattering, i.e., Kapitza resistance, reducing the mean-free path of phonon. The interface-induced thermal junctions between the MWCNTs and binder material leads to the phonon scattering phenomenon, serving as a barrier to phonon transport [27,28,32]. In addition, the high temperature environment of the specimens may reduce the phonon mean-free path. The Umklapp process, also known as phonon–phonon scattering, results in a lowering of the thermal conductivity of the specimens at high temperatures [27,32,33].

3.3. Compressive strength

The results of the compressive strength versus the exposure temperature and the MWCNT content are presented in Fig. 3 (Table A1). The trends observed in the test results according to the amount of MWCNT were similar regardless of the binder type.

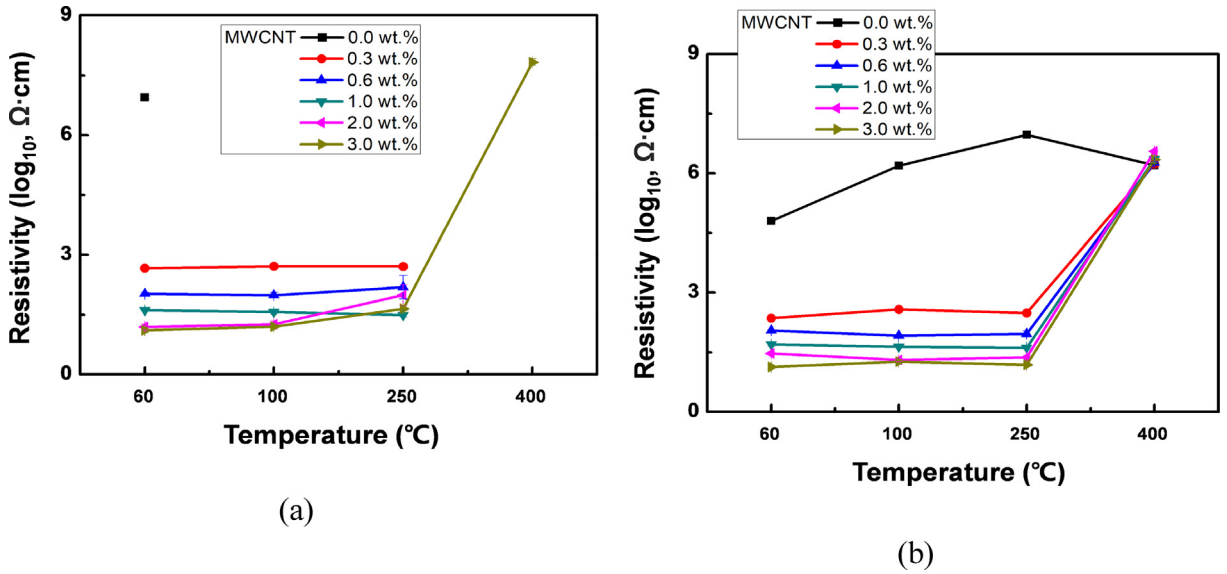

Fig. 1. Influence of the temperature and MWCNT content on the electrical resistivity of (a) PC/MWCNT and (b) AAC/MWCNT composites.

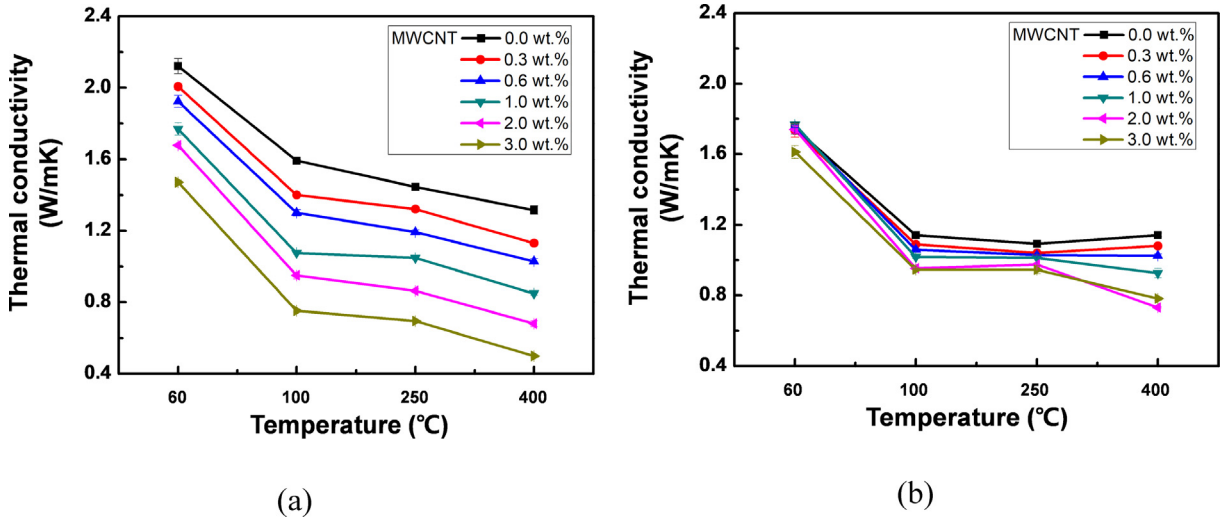

Fig. 2. Influence of the temperature and MWCNT content on the thermal conductivity of (a) PC/MWCNT and (b) AAC/MWCNT composites.

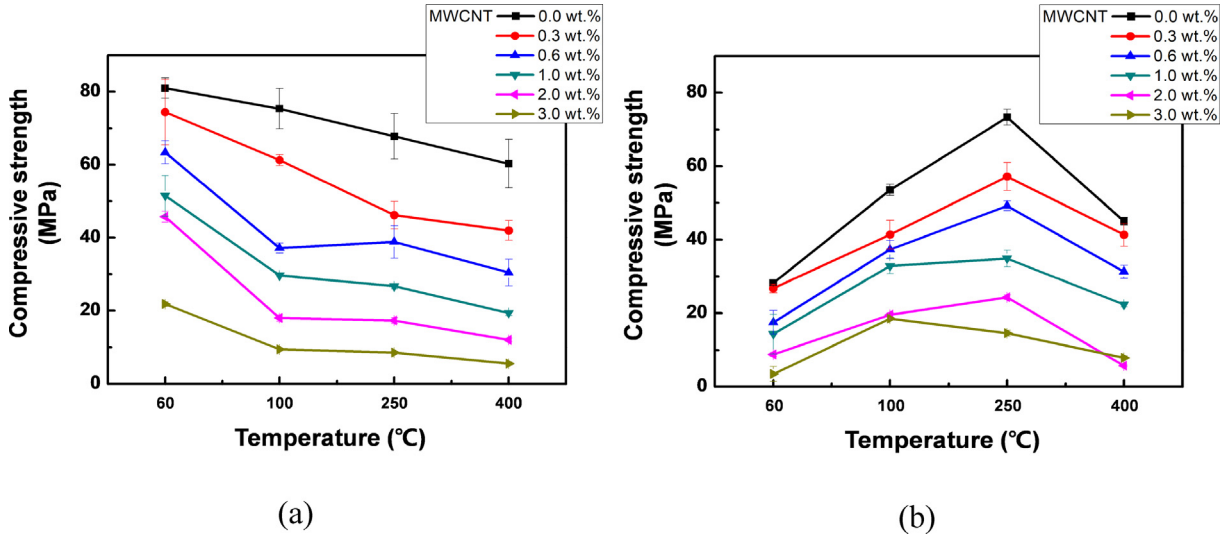

Fig. 3. Influence of the temperature and MWCNT content on the compressive strength of (a) PC/MWCNT and (b) AAC/MWCNT composites.

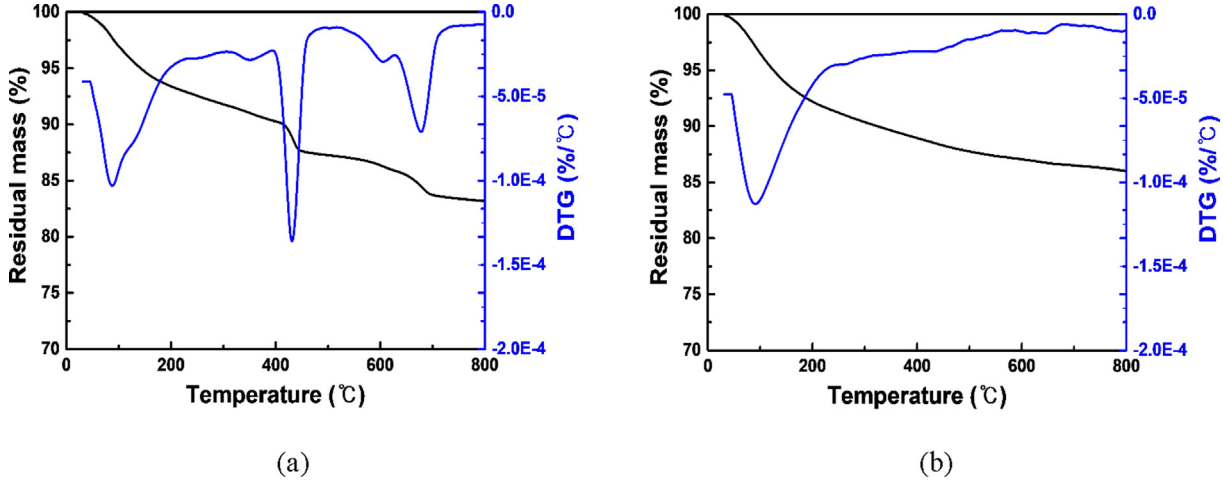

Fig. 4. Thermogravimetric analysis results of (a) PC and (b) AAC binders.

Fig. 3 (a) and (b) indicate that the compressive strength of all specimens decreased with an increase in the MWCNT content. However, the compressive strength trends of the two matrices against the temperature showed a significant difference. The PC/MWCNT composites were observed to exhibit less compressive strength as the temperatures increased regardless of the MWCNT content. On the other hand, the compressive strength of the AAC/MWCNT composites increased while the temperature increased from 60 °C to 250 °C. However, when the temperature reached 400 °C, the compressive strength of the AAC/MWCNT composites decreased, becoming similar to that at 60 °C.

It is clear that the proposed mix proportion and manufacturing process did not lead to the development of higher strength in the specimens despite the increased content of MWCNT. This occurred because the flow proposed in this study is set to be considerably higher than those in previous studies [5,13,34]. *Earlier published papers [35,36] demonstrated that the components of AAC binder started decomposing as reached exposed temperature of 400* ℃. The present study focused on enhancing the thermoelectric function of the composites rather than on increasing the compressive strength. As a result, it was found that the electrical resistivity was improved by adding MWCNT, whereas the thermal conductivity and compressive strength were decreased, showing an inversely proportional relationship with the resistivity.

In earlier work [22], the pore volume increases as the W/B ratio increases. Thus, the decrease in the compressive strength as the MWCNT amount is increased is attributed to the higher W/B and activator/binder ratios used in this work compared to those in previous studies. It is important to note that the W/B ratio of the composites (activator/binder for AAC) was increased until a desired flow was reached by the two binders (Tables 1 and 2). The PC/MWCNT composites were made with much less water due to use of a superplasticizer; therefore, it is natural for PC/MWCNT composites to exhibit higher compressive strength under the same flow conditions. A superplasticizer was not added to the AAC/MWCNT composites because the alkaline activator breaks the polymer chain of the superplasticizer, causing it to fail to perform its expected role [37,38].

3.4. Physiochemical analyses

In addition to the MWCNT content of the composite causing a substantial change in the electrical resistivity, the thermal conductivity and the compressive strength, these properties were also greatly affected by the exposure temperature and the binder matrix used. This phenomenon can be attributed to the phase evolution of the binder matrices (PC and AAC), which significantly differ in terms of their characteristics and thermal behavior.

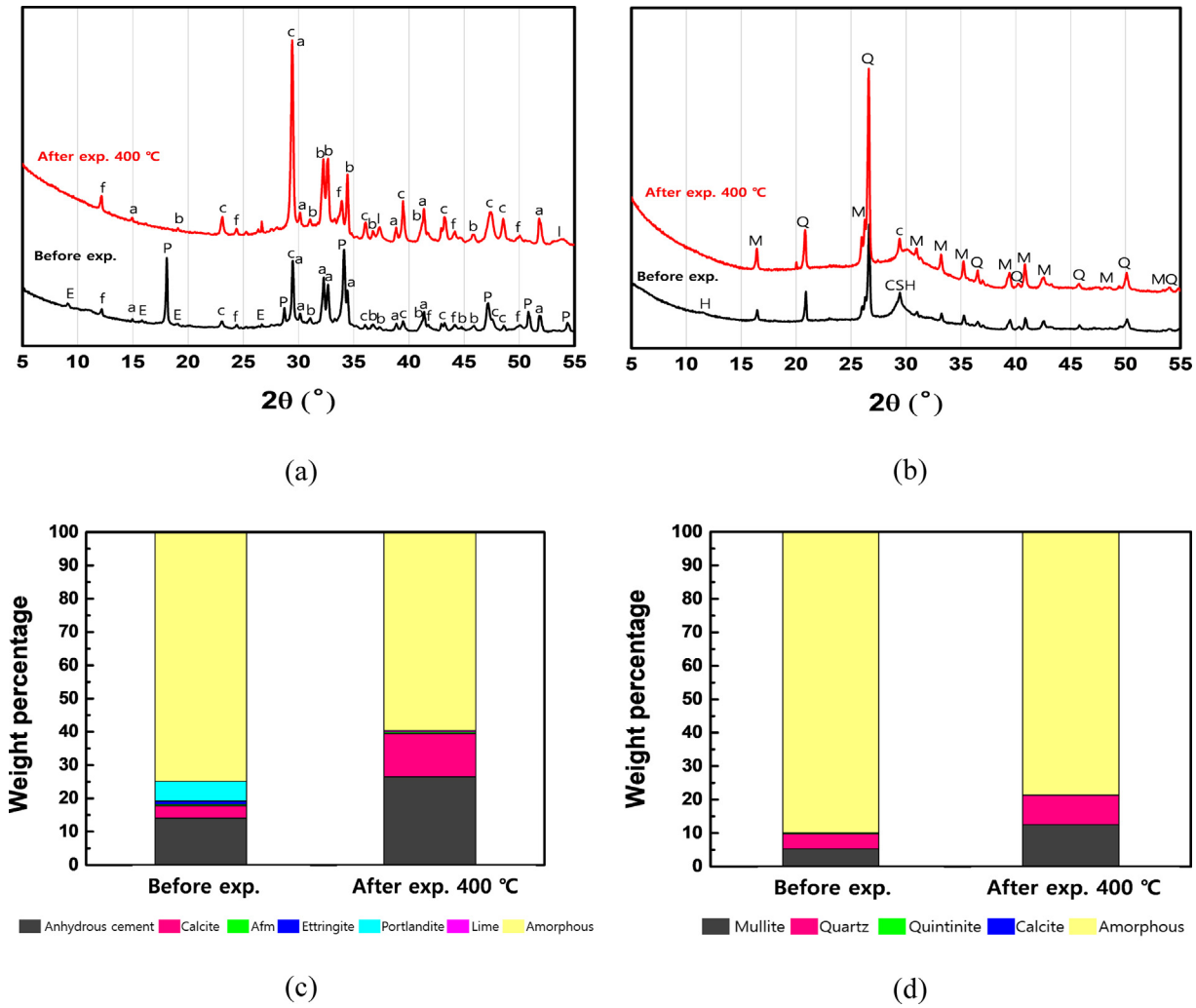

Fig. 5. X-ray diffraction patterns of (a) PC and (b) AAC, and mineralogical quantitative analysis based on Rietveld refinement for (c) PC and (d) AAC. The notations used in (a) and (b) are as follows: a-alite, b- belite, c- calcite, f- ferrite, E- ettringite, P- portlandite, M- mullite, Q- quartz, H- hydrotalcite-like phase, and CSH- C-S-H.

A series of experimental characterizations were conducted to provide more detailed information about the binder matrices, especially at elevated temperatures, and to discover the correlation with the thermoelectric properties of the composites.

The *TGA* results of the PC and AAC are shown in Fig. 4. *In the PC, the three phases at 90 °C, 430 °C, 600 °C were observed a peak by decomposition of C-S-H, $Ca(OH)_2$, $CaCO_3$ [39–41]. The DTG curve of the AAC showed peaks at 90 °C,* attributed to the dehydration of C-A-S-H [42], indicating that the thermally induced change in the binder of AAC *can be occurred* due to the evaporation of chemically and structurally bound water from the C-A-S-H gels.

The XRD pattern of the PC shown in Fig. 5(a) provides further evidence of the structural degradation in the binder material due to the thermal decomposition of ettringite and portlandite, which initially appear but then vanish at the elevated temperature. The crystallographic change in the AAC on the other hand is relatively less pronounced. Specifically, peaks due to calcite are identified, but with much less intensity in comparison with those in the

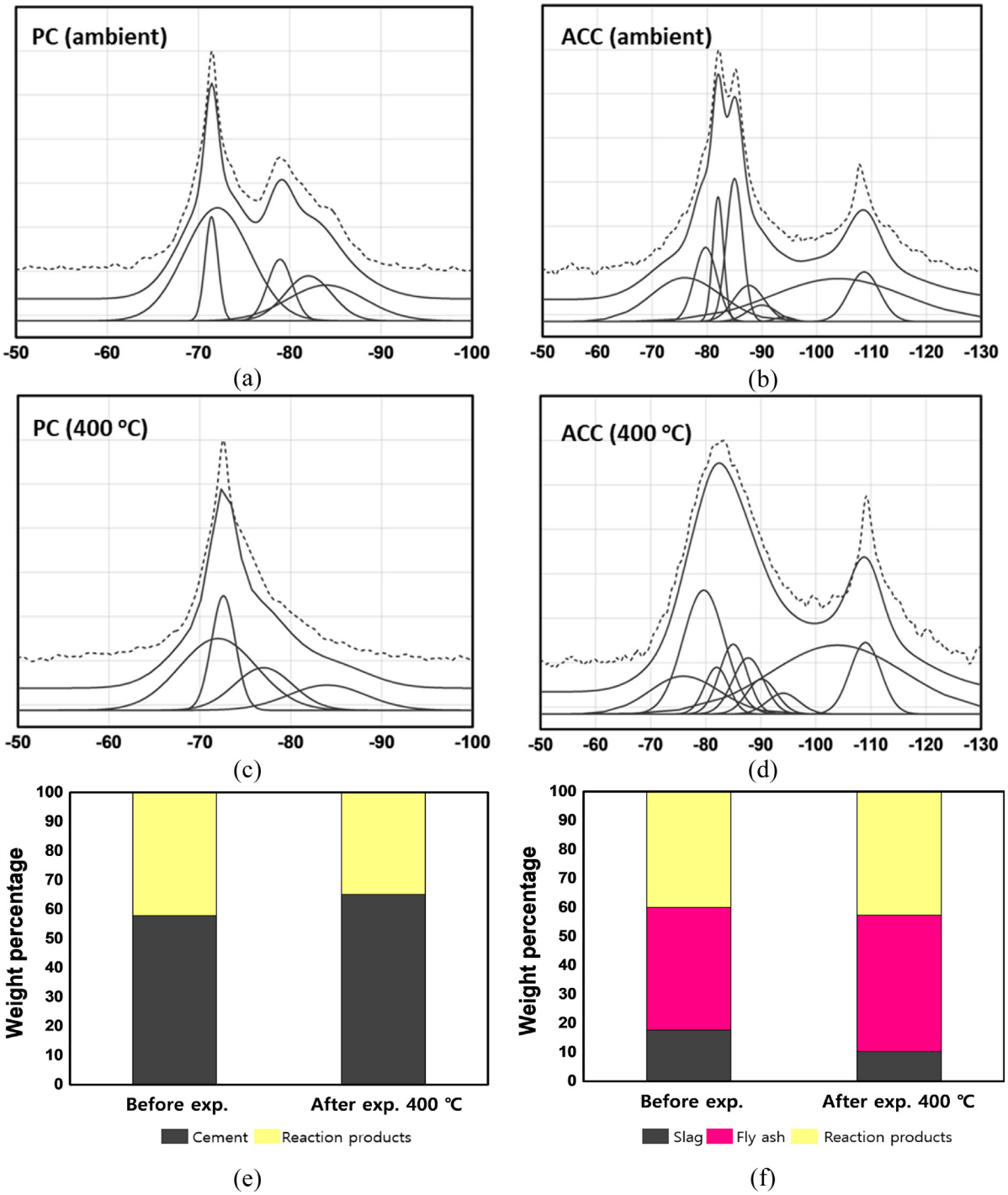

Fig. 6. ^{29}Si MAS NMR spectra of the PC and AAC: (a) and (b) present the results at an ambient temperature for the PC and AAC samples, while (c) and (d) present the results after exposure at a temperature of 400 °C. Deconvolution results are shown for comparison to show the structural changes occurring in (c) PC and (d) AAC at an elevated temperature. The experimental and simulated spectra are indicated by the dotted and solid lines, respectively, in (a)-(d).

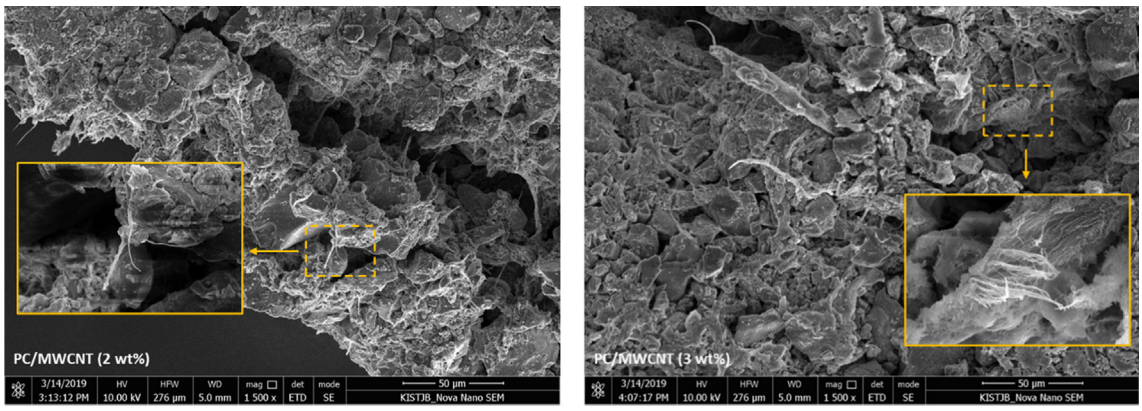

Fig. 7. SEM micrographs of (a) PC/MWCNT and (b) AAC/MWCNT composites.

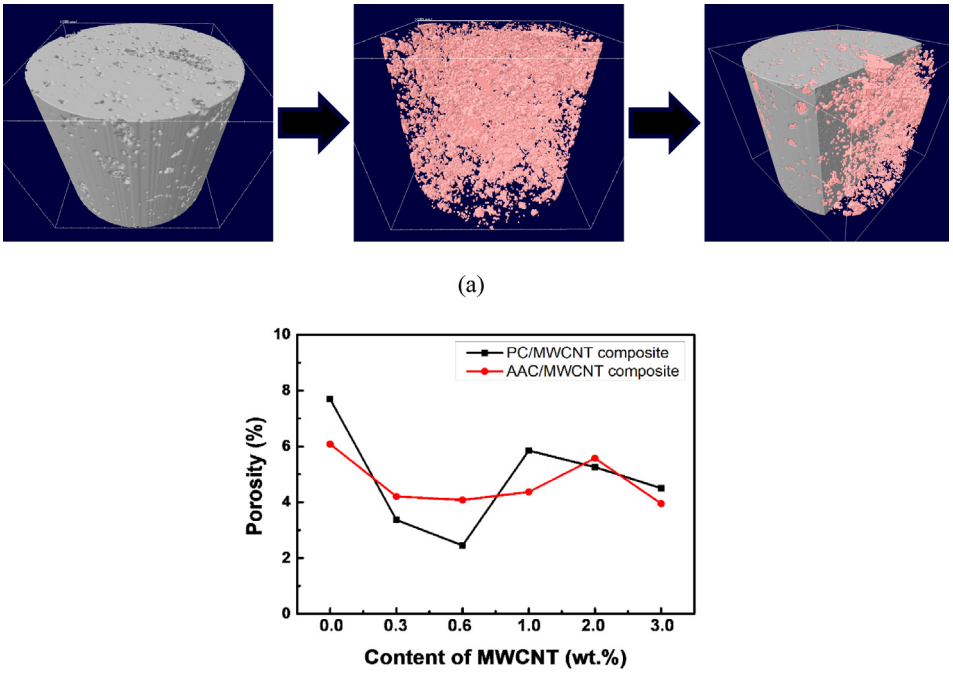

Fig. 8. Analysis of the internal structures of PC/MWCNT and AAC/MWCNT composites via micro CT: (a) typical 3D visualization of the AAC/MWCNT composite and (b) the calculated porosity value.

XRD pattern of the PC. The mineralogical quantitative information derived from the Rietveld refinement analysis shown in Fig. 5(c) and (d) suggests that both PC and AAC undergo crystallization (i.e., a reduction in the amorphous content), while the extent of crystallization is higher in the PC, which implies that the extent of the damage at the elevated temperature is likely higher in the PC. The amorphous phase in the PC mainly consists of C-S-H-type gels with a minor contribution from the AFm phases, while unreacted fly ash and GGBS, as well as C-A-S-H gels, give rise to the amorphous PC in the AAC.

The local Si environment in both the PC and AAC specimens was probed by ^{29}Si MAS NMR spectroscopy, as shown in Fig. 6, to reveal the detailed characteristic of the amorphous phase as identified by X-ray diffraction. The spectra of the PC showed resonance at around −72 ppm due to the presence of anhydrous PC clinkers of alite and belite, the intensity of which was increased by the elevated temperature. This observation together with the decreased intensity of the resonance at −77 and −84 ppm, attributed to the Q^1 and Q^2 sites in C-S-H gels, indicates that the reaction products thermally disintegrated into Q^0 structures. In addition, it can be inferred that the structural damage in the PC is not only due to the decomposition of the portlandite, AFt, and AFm phases but is also due significantly to the degradation of the C-S-H gels.

The spectra of the AAC showed resonance with a broad lineshape due to the amorphous nature of the raw fly ash and GGBS. Resonance of Q^1, Q^2, as well as Q^2(1Al) was observed in the spectra, suggesting that the dominant reaction products are C-S-H-type gels with Al substitution in the paired and bridging sites. Although this resonance due to the presence of the reaction products was reduced by the elevated temperature according to the thermogravimetric analysis and X-ray diffraction results, the thermally induced reaction of fly ash and GGBS compensated for such losses in the reaction products. This was also found in a previous study [12].

SEM micrographs of PC/MWCNT and AAC/MWCNT composites at various magnifications are presented in Fig. 7. The difference in the matrix morphologies between the PC and AAC shown in the SEM images is not noticeable. However, for the AAC sample, it can be seen that it consists of larger particles due to the fact that the unreacted slag powder is larger than the commercial PC particles. A difference from PC due to Al substitution in the slag is also observed. MWCNT showed a difference in the degree of aggrega-

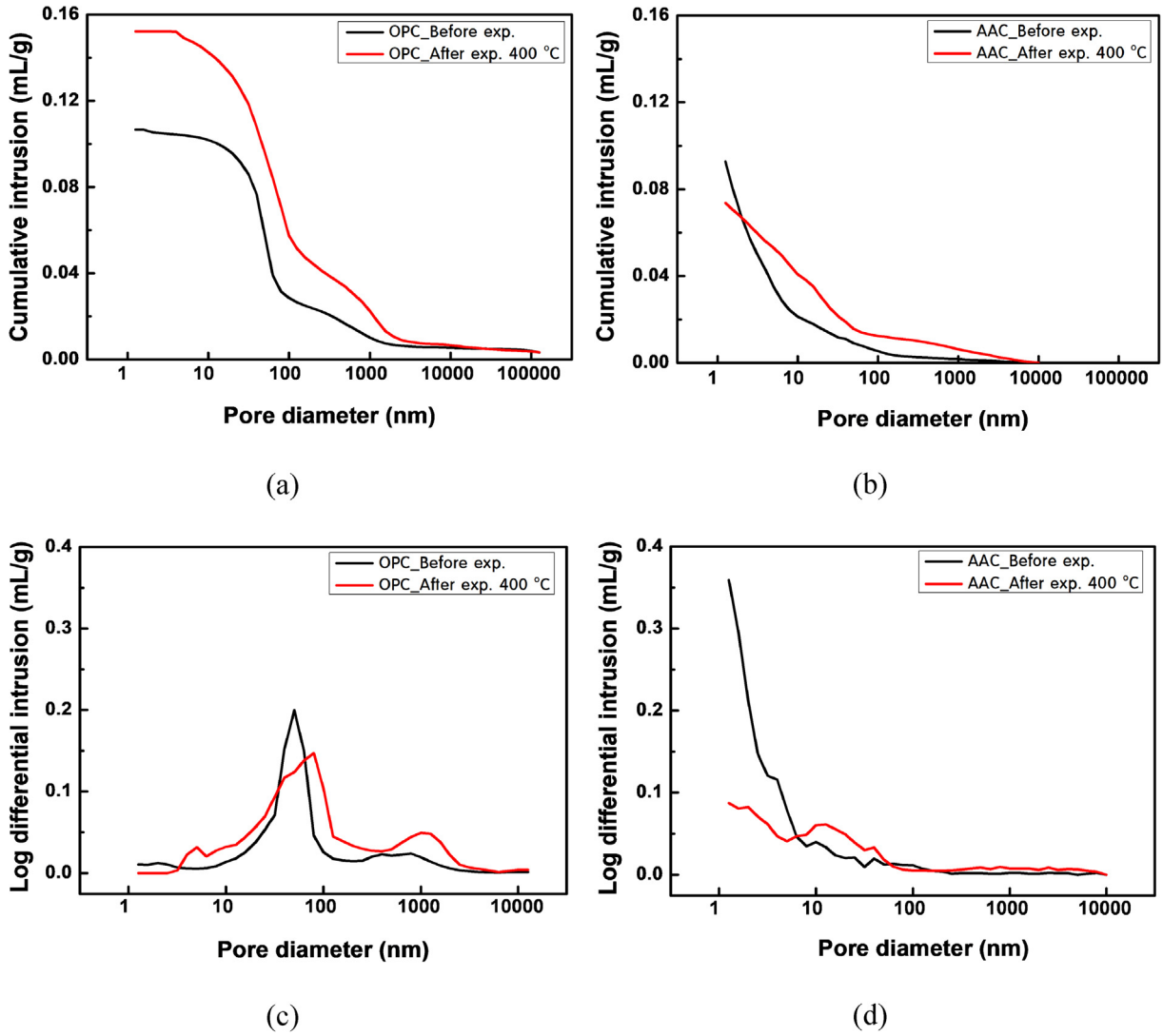

Fig. 9. Cumulative intrusion and log differential intrusion curves obtained by mercury intrusion porosimetry. The results for the OPC and AAC samples are shown in (a) and (b), and in (c) and (d), respectively.

tion according to the content. When 3.0 wt% of MWCNT was contained, a more aggregated MWCNT bundle was observed than that of 2.0 wt%.

In addition, the 3D tomography outcomes of the composites were analyzed by μ-CT, as shown in Fig. 8. It was found that the internal structure of the specimens through μ-CT showed no significant differences among the composites; therefore, the 2.0 wt% MWCNT-embedded AAC composite is presented in Fig. 8(a). The calculated porosity values according to μ-CT are shown in Fig. 8 (b). The initial porosity levels of the PC and AAC binders were approximately 8 and 6%, respectively, and they decreased with an addition of MWCNT. The decreased porosity levels were found

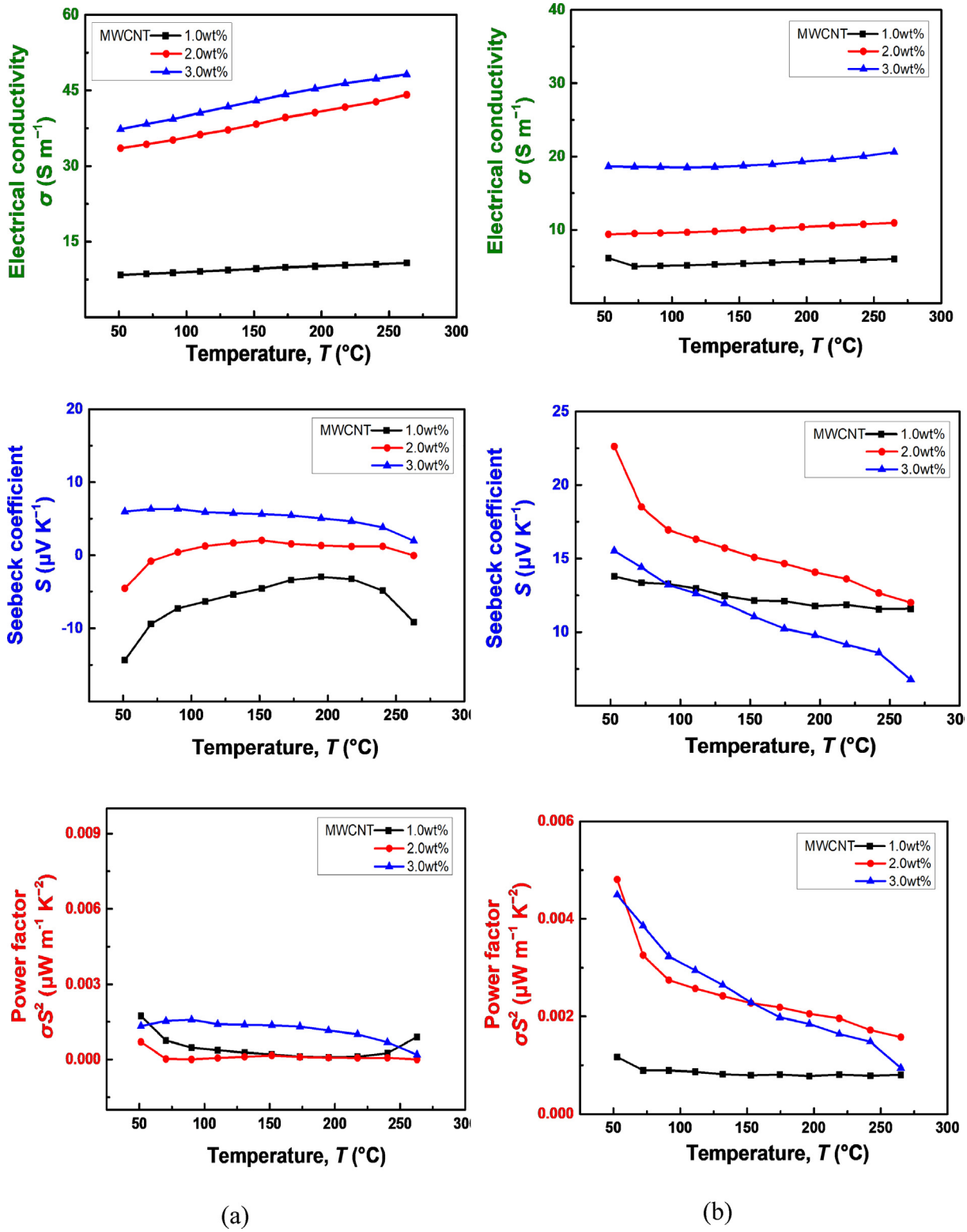

Fig. 10. Comparisons of the electrical conductivity, Seebeck coefficient, and power factor of the (a) PC/MWCNT and (b) AAC/MWCNT composites.

to increase again when the MWCNT content exceeded 0.5 wt%. Interestingly, this content is equal to the percolation threshold of the composites. It can be deduced that the nanoscale MWCNT serves to fill the pores in the composites up to a level of 0.5 wt%. However, when MWCNT is added in excess of the percolation threshold, it serves to increase the porosity due to agglomeration, interface, and dispersion issues [13]. It is also believed that this phenomenon may have a positive or negative effect on the electrical resistivity of the composites.

The MIP results of PC/MWCNT and AAC/MWCNT composites are shown in Fig. 9. This technique is very useful to observe the pore structure of a cementitious matrix. In particular, it allows one to access to the capillary pore network, which may not be accessible when using μ-CT. The cumulative intrusion of mercury into PC/MWCNT showed that there is an increase in the pore space available for mercury intrusion after exposure, suggesting increased porosity upon exposure. This was not necessarily the case for the AAC samples, with the results showing that mercury intrusion rather decreased after exposure, implying that the pore structure became complex and discontinuous under this exposure condition. This observation is also clearly reflected in the log differential intrusion curves, especially for the OPC samples, which showed an increased population of pores at approximately 1000 nm and a shift of the dominant pores to those with diameters ranging from approximately 50 nm to 70 nm. On the other hand, the log differential intrusion curves of the AAC samples showed no distinctive change upon exposure, implying that the pore structures of these samples are less affected by a thermal gradient in comparison with the OPC samples.

3.5. Thermoelectric characteristics

The temperature dependency characteristics of the electrical conductivity, Seebeck coefficient, and power factor characteristics are plotted in Fig. 10 *(a)*. Note that the composites with low electrical conductivity, i.e., a MWCNT amount less than 1.0 wt%, were not measurable. Fig. 9 (a) and (b) show that electrical conductivity of all specimens increases with an increase in the MWCNT content. In all cases, PC showed better electrical conductivity than AAC when the same amount of MWCNT was incorporated. This is attributed to the better dispersion of MWCNT given the use of the superplasticizer [13,38].

Overall, the AAC/MWCNT composites were found to have a higher Seebeck coefficient than the PC/MWCNT composites. For

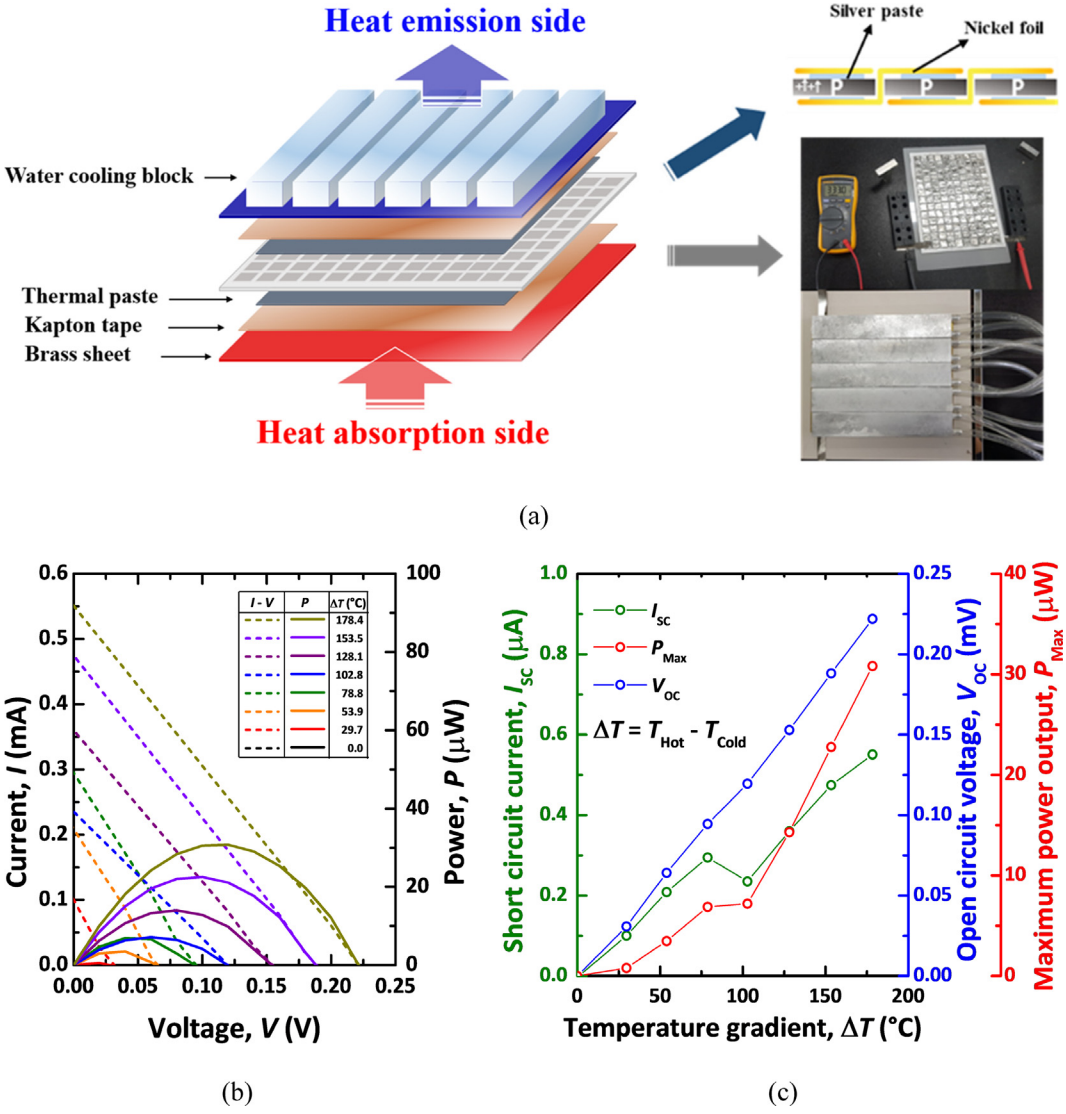

Fig. 11. (a) Schematic design of the AAC/MWCNT module, (b) relationship between the current–voltage and power-voltage characteristics for the AAC/MWCNT module, and (c) variation of the short-circuit current, open-circuit voltage, and maximum power output as a function of the temperature gradient.

the PC/MWCNT composites, the performance of the Seebeck coefficient gradually increased as the MWCNT content was increased, whereas the AAC/MWCNT composites were observed to have the highest value when MWCNT was incorporated at a rate of 2.0 wt%. When 3.0 wt% of MWCNT is incorporated into AAC, the result is rather worse, with the highest Seebeck coefficient of 22.6263 μVK^{-1} obtained for AAC/MWCNT composites with MWCNT at a rate of 2.0 wt% at an exposure temperature of 50 °C.

The addition of MWCNT to the PC did not have much of an effect on the thermoelectric properties, as shown in Fig. 10 *(a)*. However, it was observed that the addition of more than 2.0 wt% MWCNT to AAC resulted in a considerably enhanced power factor. The AAC composite containing 3.0 wt% of MWCNT did not show a significant difference compared to when 2.0 wt% was added. The highest value of the power factor is 0.0048 $Wm^{-1}K^{-2}$ for the AAC/MWCNT composites with MWCNT at 2.0 wt% at a temperature of 50 °C.

3.6. Thermoelectric module

A thermoelectric module was also fabricated to evaluate the energy production capacity of the proposed specimen. Based on the present experimental results, it was considered that AAC as a binder would have a greater effect on improving the thermoelectric performance. In addition, the ideal content of MWCNT was determined to be 2.0 wt%. The schematic diagram of the AAC/MWCNT thermoelectric module used in this study is exhibited in Fig. 11(a). The manufacturing procedure is described in Fig. 11 (a). A detailed sketch of the present thermoelectric module is also shown in Fig. A1.

The electrical characteristics of the AAC/MWCNT module at the temperature gradients used here are summarized in Fig. 11(b) and (c). Fig. 11(b) shows the variation of the current–voltage and power-voltage characteristics with temperature differences between the hot and cold side (ΔT). It was observed that the electrical characteristics of the present thermoelectric module were improved when increasing ΔT. Fig. 11(c) presents the variations of the short-circuit current (I_{SC}), maximum power output (P_{max}) with the temperature gradient, and open-circuit voltage (V_{OC}).

It can be seen that the open-circuit voltage and short-circuit current increase with an increase of the temperature. The open-circuit voltage and power output were related to the temperature difference between the hot junction and the cold junction of the thermoelectric module. Regarding the temperature of the heat-emission and heat-absorption sides, in this case T_{hot} = 200 °C and T_{cold} = 21.6 °C (ΔT = 178.4 °C), the thermoelectric module produces a maximum power output value of 30.83 μW.

4. Conclusions

Here, we studied various physiochemical properties, specifically the thermoelectric behavior of MWCNT-incorporated PC and AAC composites. MWCNT-incorporated PC and AAC composites were fabricated at various mix proportions and were exposed to different temperatures to investigate the effects of both parameters on the material characteristics of the composite. According to the results, the AAC/MWCNT composite has good electrical and mechanical properties when exposed to a high temperature. It is considered that the AAC/MWCNT composite is more suitable as a thermoelectric material than the PC/MWCNT composite, as the electrical and thermal properties are directly affected by the thermoelectric characteristics. The main results of the present study are summarized below:

(1) The electrical resistivity of both the MWCNT-incorporated PC and AAC composites did not change from 60 to 250 °C, but they increased significantly at 400 °C. In addition, the electrical resistivity of all specimens decreased as the MWCNT content was increased, while that of samples with MWCNT exceeding 2.0 wt% did not significantly decrease.
(2) The thermal conductivity of all specimens decreased with an increase in the MWCNT content and the exposure temperature. It is considered that the MWCNTs dispersed in the PC/MWCNT and AAC/MWCNT composites could cause interface scattering, i.e., Kapitza resistance. In addition, phonon–phonon scattering was found to lower the thermal conductivity of the specimens at high temperatures.
(3) The compressive strength of the PC/MWCNT composites decreased with an increase in the MWCNT content and at higher exposure temperature. However, the compressive strength of the AAC/MWCNT composites increased when the temperature was increased from 60 to 250 °C, and that of all specimens decreased with an increase of the MWCNT content.
(4) *The highest value of the Seebeck coefficient was obtained with an AAC/MWCNT composites with MWCNT incorporated at a rate of 2.0 wt%.*
(5) *The thermoelectric module produces a maximum power output of* 30.83 μW *when* $T_{hot} = 200\,°C$ *and* $T_{cold} = 21.6\,°C$ ($\Delta T = 178.4\,°C$).

CRediT authorship contribution statement

Hyeong Min Park: Writing - original draft, Conceptualization, Methodology. **Solmoi Park:** Data curation, Investigation. **In-Jin Shon:** Data curation. **G.M. Kim:** Visualization, Methodology. **Sun-bin Hwang:** Validation, Formal analysis. **Min Wook Lee:** Writing - review & editing. **Beomjoo Yang:** Writing - review & editing, Supervision.

Declaration of Competing Interest

The authors declare that they have no known competing financial interests or personal relationships that could have appeared to influence the work reported in this paper.

Acknowledgement

This study was supported by the National Research Foundation of Korea (NRF) grant funded by the Korea government (MSIT) (2020R1C1C1005063) and by the Korean National Police Agency. [Project Name: Development of on-site support equipment for criminal safety arrest / Project Number: PR08-01-000-20]. In addition, this research was supported by the Basic Research Project of the Korea Institute of Geoscience and Mineral resources (KIGAM) funded by the Ministry of Science, ICT and Future Planning of Korea (GP2020-021).

Appendix A

Fig. A1. Additional information of the size of the fabricated thermoelectric module with 130 elements. A size of mold (PPS, Polyphenylene Sulfide) was selected in consideration of the maximum size applicable to the hot plate, and the size and thickness of the specimen considered the easy level for casting. The fabricated module consists of a sandwich structure with thermal paste, brass sheet, and kapton tape. Thermal paste was applied to the uneven surface of each specimen for uniform heat absorption and emission. The brass sheet was used to prevent damage due to direct bonded between the thermal paste and the hot plate. In addition, Kapton tape was attached to prevent a short circuit

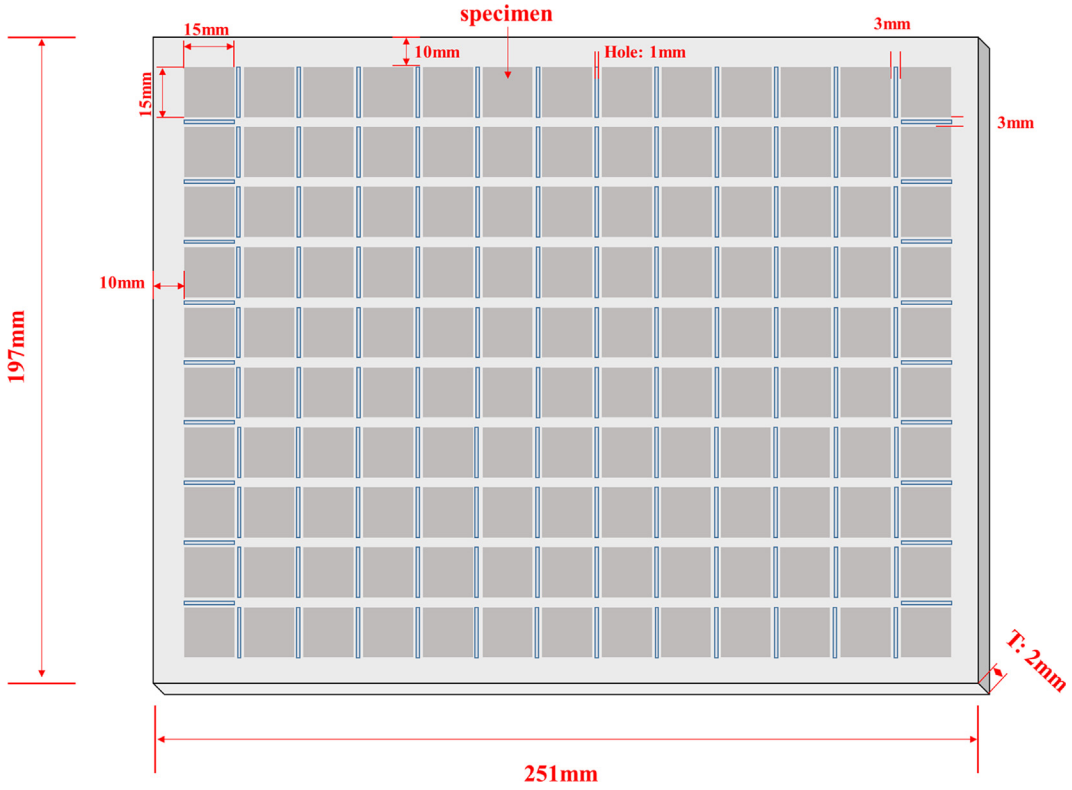

Fig. A1. A sketch of thermoelectric module.

Table A1
Raw values of measurement data illustrated in Figs. 1–3.

Specimen	Curing temperature (°C)	Resistivity (Ω·cm)	Thermal conductivity (W/mk)	Compressive strength(MPa)
C-0	60	0.044	0.042	2.785
	100	–	0.007	5.567
	250	–	0.004	6.273
	400	–	0.024	6.671
C-0.3C	60	0.018	0.015	8.976
	100	0.035	0.008	1.501
	250	0.015	0.014	3.748
	400	–	0.014	2.708
C-0.6C	60	0.038	0.034	3.157
	100	0.074	0.018	1.339
	250	0.293	0.012	4.437
	400	–	0.015	3.615
C-1.0C	60	0.010	0.034	5.584
	100	0.056	0.007	0.301
	250	0.052	0.010	0.710
	400	–	0.011	0.729
C-2.0C	60	0.077	0.009	1.508
	100	0.084	0.019	0.892
	250	0.257	0.011	0.775
	400	–	0.016	0.443
C-3.0C	60	0.068	0.012	0.628
	100	0.020	0.007	0.383
	250	0.090	0.007	0.431
	400	0.088	0.008	0.442
AAC-0	60	0.017	0.033	0.685
	100	0.003	0.008	1.523
	250	0.013	0.017	2.178
	400	0.035	0.011	1.111
AAC-0.3C	60	0.029	0.038	1.168
	100	0.017	0.004	3.887
	250	0.028	0.011	3.791
	400	0.077	0.014	3.043
AAC-0.6C	60	0.012	0.007	3.235
	100	0.017	0.006	2.429
	250	0.078	0.004	1.367
	400	0.024	0.009	1.789

(*continued on next page*)

Table A1 (*continued*)

Specimen	Curing temperature (°C)	Resistivity (Ω·cm)	Thermal conductivity (W/mk)	Compressive strength(MPa)
AAC-1.0C	60	0.043	0.007	5.396
	100	0.015	0.010	2.095
	250	0.030	0.005	2.276
	400	0.030	0.027	0.579
AAC-2.0C	60	0.038	0.022	0.525
	100	0.038	0.006	0.636
	250	0.041	0.001	0.691
	400	0.016	0.003	0.141
AAC-3.0C	60	0.049	0.037	2.097
	100	0.023	0.001	0.354
	250	0.028	0.022	0.836

Table A2
Mix proportion of AAC/MWCNT composite (vol.%).

Specimen	Slag	Fly ash	MWCNT	Alkali activator	Flow (mm)
AAC-0	416.67	925.93	0.0	0.86	111.5 ± 11.5
AAC-0.3C			0.2	0.91	
AAC-0.6C			0.3	0.99	
AAC-1.0C			0.6	1.08	
AAC-2.0C			1.1	1.29	
AAC-3.0C			1.7	1.51	

Table A3
Mix proportion of cement/MWCNT composite (vol.%).

Specimen	Cement	MWCNT	Water	Superplasticizer	Flow (mm)
C-0	317.46	0.0	0.26	13.33	112.5 ± 12.5
C-0.3C		0.2	0.3		
C-0.6C		0.3	0.35		
C-1.0C		0.6	0.46		
C-2.0C		1.1	0.61		
C-3.0C		1.7	0.8		

between the specimen and brass sheet. Each specimen was constructed with an electrically conductive layer by contacting the nickel foil to induce the current flow.

Tables A1-A3. Raw data for providing additional information on resistivity, thermal conductivity, and compressive strength shown in Figs. 1-3.

References

[1] K.P. Mehta, Reducing the environmental impact of concrete, Concr. Int. 23 (10) (2001) 61–66.
[2] V. Malhotra, Introduction: sustainable development and concrete technology, Concr. Int. 24 (7) (2002).
[3] R. Snellings, G. Mertens, J. Elsen, Supplementary cementitious materials, Rev. Miner. Geochem. 74 (1) (2012) 211–278.
[4] I.W. Nam, H.K. Kim, H.K. Lee, Influence of silica fume additions on electromagnetic interference shielding effectiveness of multi-walled carbon nanotube/cement composites, Constr. Build. Mater. 30 (2012) 480–487.
[5] H.K. Kim, I.S. Park, H.K. Lee, Improved piezoresistive sensitivity and stability of CNT/cement mortar composites with low water–binder ratio, Compos. Struct. 116 (2014) 713–719.
[6] J. Wei, Y. Fan, L. Zhao, F. Xue, L. Hao, Q. Zhang, Thermoelectric properties of carbon nanotube reinforced cement-based composites fabricated by compression shear, Ceram. Int. 44 (6) (2018) 5829–5833.
[7] L. Tzounis, M. Liebscher, R. Fuge, A. Leonhardt, V. Mechtcherine, P-and n-type thermoelectric cement composites with CVD grown p-and n-doped carbon nanotubes: Demonstration of a structural thermoelectric generator, Energy Build. 191 (2019) 151–163.
[8] I.M. Low, in: Advances in Ceramic Matrix Composites, Elsevier, 2018, pp. 1–7, https://doi.org/10.1016/B978-0-08-102166-8.00001-3.
[9] N.K. Lee, H.K. Lee, Setting and mechanical properties of alkali-activated fly ash/slag concrete manufactured at room temperature, Constr. Build. Mater. 47 (2013) 1201–1209.
[10] G. Fang, W.K. Ho, W. Tu, M. Zhang, Workability and mechanical properties of alkali-activated fly ash-slag concrete cured at ambient temperature, Constr. Build. Mater. 172 (2018) 476–487.
[11] J. Xie, J. Wang, R. Rao, C. Wang, C. Fang, Effects of combined usage of GGBS and fly ash on workability and mechanical properties of alkali activated geopolymer concrete with recycled aggregate, Compos. B Eng. 164 (2019) 179–190.
[12] S.M. Park, J.G. Jang, N.K. Lee, H.K. Lee, Physicochemical properties of binder gel in alkali-activated fly ash/slag exposed to high temperatures, Cem. Concr. Res. 89 (2016) 72–79.
[13] G.M. Kim, B.J. Yang, K.J. Cho, E.M. Kim, H.K. Lee, Influences of CNT dispersion and pore characteristics on the electrical performance of cementitious composites, Compos. Struct. 164 (2017) 32–42.
[14] G.M. Kim, S.M. Park, G.U. Ryu, H.K. Lee, Electrical characteristics of hierarchical conductive pathways in cementitious composites incorporating CNT and carbon fiber, Cem. Concr. Compos. 82 (2017) 165–175.
[15] G.M. Kim, I.W. Nam, B. Yang, H.N. Yoon, H.K. Lee, S. Park, Carbon nanotube (CNT) incorporated cementitious composites for functional construction materials: The state of the art, Compos. Struct. 227 (2019) 111244, https://doi.org/10.1016/j.compstruct.2019.111244.
[16] G.M. Kim, B.J. Yang, G.U. Ryu, H.K. Lee, The electrically conductive carbon nanotube (CNT)/cement composites for accelerated curing and thermal cracking reduction, Compos. Struct. 158 (2016) 20–29.
[17] I.W. Nam, H.K. Lee, Synergistic effect of MWNT/fly ash incorporation on the EMI shielding/absorbing characteristics of cementitious materials, Constr. Build. Mater. 115 (2016) 651–661.
[18] G.M. Kim, B.J. Yang, H.N. Yoon, H.K. Lee, Synergistic effects of carbon nanotubes and carbon fibers on heat generation and electrical characteristics of cementitious composites, Carbon 134 (2018) 283–292.
[19] J. Péra, J. Ambroise, M. Chabannet, Properties of blast-furnace slags containing high amounts of manganese, Cem. Concr. Res. 29 (2) (1999) 171–177.
[20] J. Zhang, C. Shi, Z. Zhang, Effect of Na2O concentration and water/binder ratio on carbonation of alkali-activated slag/fly ash cements, Constr. Build. Mater. 269 (2021) 121258.
[21] I. Mehdipour, K.H. Khayat, Effect of particle-size distribution and specific surface area of different binder systems on packing density and flow characteristics of cement paste, Cem. Concr. Compos. 78 (2017) 120–131.

[22] H.M. Park, G.M. Kim, S.Y. Lee, H. Jeon, S.Y. Kim, M. Kim, J.W. Kim, Y.C. Jung, B.J. Yang, Electrical resistivity reduction with pitch-based carbon fiber into multi-walled carbon nanotube (MWCNT)-embedded cement composites, Constr. Build. Mater. 165 (2018) 484–493.
[23] H. Yoon, D. Jang, H.-K. Lee, I. Nam, Influence of carbon fiber additions on the electromagnetic wave shielding characteristics of CNT-cement composites, Constr. Build. Mater. 269 (2021) 121238.
[24] I.W. Nam, H. Souri, H.K. Lee, Percolation threshold and piezoresistive response of multi-wall carbon nanotube/cement composites, Smart Struct. Syst. 18 (2) (2016) 217–231.
[25] Y.N. Chan, X. Luo, W. Sun, Compressive strength and pore structure of high-performance concrete after exposure to high temperature up to 800 C, Cem. Concr. Res. 30 (2) (2000) 247–251.
[26] S. Park, J. Seo, H. Lee, Thermal evolution of hydrates in carbonation-cured Portland cement, Mater. Struct. 51 (1) (2018) 7.
[27] K. Ahmad, P. Wei, C. Wan, Thermal conductivities of alumina-based multiwall carbon nanotube ceramic composites, J. Mater. Sci. 49 (17) (2014) 6048–6055.
[28] S. Berber, Y.-K. Kwon, D. Tománek, Unusually high thermal conductivity of carbon nanotubes, Phys. Rev. Lett. 84 (20) (2000) 4613–4616.
[29] J. Hone, M.C. Llaguno, M.J. Biercuk, A.T. Johnson, B. Batlogg, Z. Benes, J.E. Fischer, Thermal properties of carbon nanotubes and nanotube-based materials, Appl. Phys. A 74 (3) (2002) 339–343.
[30] Q. Huang, L. Gao, Y. Liu, J. Sun, Sintering and thermal properties of multiwalled carbon nanotube–BaTiO 3 composites, J. Mater. Chem. 15 (20) (2005) 1995–2001.
[31] H.-L. Zhang, J.-F. Li, B.-P. Zhang, K.-F. Yao, W.-S. Liu, H. Wang, Electrical and thermal properties of carbon nanotube bulk materials: Experimental studies for the 328–958 K temperature range, Phys. Rev. B 75 (20) (2007) 205407.
[32] G.D. Zhan, A.K. Mukherjee, Carbon nanotube reinforced alumina-based ceramics with novel mechanical, electrical, and thermal properties, Int. J. Appl. Ceram. Technol. 1 (2) (2004) 161–171.
[33] L. Challis, L.J. Challis, Electron-Phonon Interactions in Low-Dimensional Structures, Oxford University Press on Demand, 2003.
[34] F. Naeem, H.K. Lee, H.K. Kim, I.W. Nam, Flexural stress and crack sensing capabilities of MWNT/cement composites, Compos. Struct. 175 (2017) 86–100.
[35] W. Dong, W. Li, K. Wang, B. Han, D. Sheng, S.P. Shah, Investigation on physicochemical and piezoresistive properties of smart MWCNT/cementitious composite exposed to elevated temperatures, Cem. Concr. Compos. 112 (2020) 103675.
[36] J. Seo, S. Bae, D. Jang, S. Park, B. Yang, H.-K. Lee, Thermal behavior of alkali-activated fly ash/slag with the addition of an aerogel as an aggregate replacement, Cem. Concr. Compos. 106 (2020) 103462.
[37] J.G. Jang, N.K. Lee, H.K. Lee, Fresh and hardened properties of alkali-activated fly ash/slag pastes with superplasticizers, Constr. Build. Mater. 50 (2014) 169–176.
[38] G.M. Kim, I.W. Nam, H.N. Yoon, H.K. Lee, Effect of superplasticizer type and siliceous materials on the dispersion of carbon nanotube in cementitious composites, Compos. Struct. 185 (2018) 264–272.
[39] W. Deboucha, N. Leklou, A. Khelidj, M.N. Oudjit, Hydration development of mineral additives blended cement using thermogravimetric analysis (TGA): Methodology of calculating the degree of hydration, Constr. Build. Mater. 146 (2017) 687–701.
[40] J.G. Jang, H.J. Kim, S.M. Park, H.K. Lee, The influence of sodium hydrogen carbonate on the hydration of cement, Constr. Build. Mater. 94 (2015) 746–749.
[41] S. Kourounis, S. Tsivilis, P.E. Tsakiridis, G.D. Papadimitriou, Z. Tsibouki, Properties and hydration of blended cements with steelmaking slag, Cem. Concr. Res. 37 (6) (2007) 815–822.
[42] S.A. Bernal, E.D. Rodríguez, R. Mejía de Gutiérrez, M. Gordillo, J.L. Provis, Mechanical and thermal characterisation of geopolymers based on silicate-activated metakaolin/slag blends, J. Mater. Sci. 46 (16) (2011) 5477–5486.